Organic Electronics 14 (2013) 2582–2589

Contents lists available at SciVerse ScienceDirect

Organic Electronics

journal homepage: www.elsevier.com/locate/orgel

H-aggregation mode in triple-decker phthalocyaninato-europium semiconductors. Materials design for high-performance air-stable ambipolar organic thin film transistors

Dapan Li [a], Hailong Wang [b], Jinglan Kan [b], Wenjing Lu [a], Yanli Chen [a,*], Jianzhuang Jiang [b,*]

[a] Shandong Provincial Key Laboratory of Fluorine Chemistry and Chemical Materials, School of Chemistry and Chemical Engineering, University of Jinan, Jinan 250022, PR China

[b] Beijing Key Laboratory for Science and Application of Functional Molecular and Crystalline Materials, Department of Chemistry, University of Science and Technology Beijing, Beijing 100083, PR China

ARTICLE INFO

Article history:
Received 14 June 2013
Received in revised form 3 July 2013
Accepted 4 July 2013
Available online 18 July 2013

Keywords:
Ambipolar
OTFT
H-aggregation
Phthalocyanine
Triple-decker

ABSTRACT

Two new tris(phthalocyaninato) europium complexes $Eu_2(Pc)[Pc(OPh)_8]_2$ (**1**) and $Eu_2[Pc(OPh)_8]_3$ (**2**) [Pc = unsubstituted phthalocyaninate; $Pc(OPh)_8$ = 2,3,9,10,16,17,23,24-octaphenoxyphthalocyaninate], were designed and synthesized. Introduction of different number of electron-withdrawing phenoxy substituents at the phthalocyanine periphery within the triple-decker complexes not only ensures their good solubility in conventional organic solvents, but more importantly successfully tunes their HOMO and LUMO levels into the range of air-stable ambipolar organic semiconductor required on the basis of electrochemical studies over both **1** and **2**, meanwhile fine controlling of aggregation mode (*H* vs. *J*) in solution-based film for improving OTFT performance is also achieved. Measurements over the OTFT devices fabricated from these sandwich compounds by a solution-based quasi–Langmuir–Shäfer (QLS) method reveal their ambipolar semiconductor nature associated with suitable HOMO and LUMO energy levels. Due to the *H*-aggregation mode employed by the heteroleptic triple-decker molecules in the QLS film, excellent performances with the electron and hole mobility in air as high as 0.68 and 0.014 $cm^2 V^{-1} s^{-1}$, respectively, have been revealed for the OTFT devices of heteroleptic triple-decker **1**. This represents the best performance so far for solution-processable ambipolar single-component phthalocyanine-based OTFTs obtained under ambient conditions. In good contrast, homoleptic analogue **2** prefers to *J*-type aggregation and this results in relatively lower electron and hole mobility, around 0.041 and 0.0026 $cm^2 V^{-1} s^{-1}$ in air, respectively, for the devices fabricated. In particular, the performance of the devices fabricated based on **1** was found to remain almost unchanged in terms of both the carrier mobilities and on/off ratio even after being stored under ambient for 4 months.

1. Introduction

The development of solution-processable thin-film transistors based on organic semiconductors (OTFTs) exhibiting high carrier mobility and good ambient stability is crucial to realizing low-cost and mechanically flexible printed electronics [1–4]. During the past decade, intensive researches towards developing novel semiconductor materials especially those possessing π-conjugated electronic structure including conjugated polymers, oligomeric thiophenes, linear fused acenes, perylenes, and phthalocyanines have yielded a number of unipolar transistors with either hole or electron as the sole charge carrier [5–14]. However, ambipolar OTFTs which allow dual operation of

* Corresponding authors. Tel.: +86 053189736150 (Y. Chen).
E-mail addresses: chm_chenyl@ujn.edu.cn (Y. Chen), jianzhuang@ustb.edu.cn (J. Jiang).

1566-1199/$ - see front matter © 2013 Elsevier B.V. All rights reserved.
http://dx.doi.org/10.1016/j.orgel.2013.07.003

both *p* and *n* types are highly desired for practical application in integrated circuits like high gain complementary metal-oxide-semiconductor inverters and light emitting devices [15–19]. Since the first demonstration of ambipolar charge transport in a bilayer OTFT of small-molecule semiconductors [20], various approaches including blending two organic components [21], modifying gate insulator or electrodes [22,23], and single-component organic molecular semiconductors [24–27] have been developed for the purpose of realizing the ambipolar OTFTs. Among which the realization of implementing organic complementary circuitry using a single molecular semiconductor rather than two different materials is very important due to the significantly simplified device fabrication. As a result, design and synthesis of soluble ambipolar organic semiconductors with acceptable performance and robust air stability has become the pivotal prerequisite advancing from emerging prototypes to the wide range of applications of organic semiconductor. Extensive investigation revealed the crucial characteristics of ambipolar single-component organic semiconductors in high-performance, air-stable, solution-processable OTFTs including suitable frontier molecular orbital (FMO) energies and long-range molecular ordering in solution-processed film [24–30]. For organic semiconductors with conjugated electronic structure, the energy of the lowest unoccupied molecular orbitals (LUMOs), that are necessary for ensuring effective electron injection and stable electron transport under ambient conditions, should locate below −4.0 eV, while that of the highest occupied molecular orbitals (HOMOs) should align with the work function of air-stable electrodes (Au: 5.1 eV) for the purpose of diminishing the hole injection barrier [24–27]. However, searching for good ambipolar organic semiconductors with suitable HOMO and LUMO energies and meanwhile delicate balance between solubility in conventional organic solvents and efficient molecular packing behavior in solid state still remains a great challenge in this field.

Among various organic semiconductors, phthalocyanines have emerged as the important one due to their unique electronic characteristics, high chemical, thermal, and electrochemical stability as well as the easy tuning their optical and electronic properties by introducing appropriate peripheral substituents and central metal ions [31–33]. As early as 1990, the sandwich-type bis(phthalocyaninato) rare earth double-decker complexes (MPc_2, M = Tm, Lu) were revealed to be promising ambipolar organic architecture for OTFTs by Guillaud and co-workers [34]. This was verified by the late demonstration of high-mobility ambipolar organic semiconducting properties of sandwich-type tris(phthalocyaninato) rare earth triple-decker complexes bringing peripheral electron-withdrawing substituents [35]. To better understand and further improve the performance of sandwich-type phthalocyaninato rare earth semiconductors, establishment of the in-depth structure-property correlations appears to be necessary. As part of our continuous effort towards the fabrication of high-performance, solution processable, air-stable single-phthalocyanine component based ambipolar OTFTs, in the present paper we describe the design and preparation of two new tris(phthalocyaninato) europium complexes $Eu_2(Pc)[Pc(OPh)_8]_2$ (**1**) and $Eu_2[Pc(OPh)_8]_3$ (**2**) [Pc = unsubstituted phthalocyaninate; $Pc(OPh)_8$ = 2,3,9, 10,16,17,23, 24-octaphenoxyphthalocyaninate], Scheme 1. Introduction of different number of electron-withdrawing phenoxy substituents at the phthalocyanine periphery within the triple-decker complexes not only ensures their good solubility in conventional organic solvents [36,37], but more importantly successfully tunes their LUMO and HOMO levels into the range of air-stable ambipolar organic semiconductors required on the basis of electrochemical studies over both **1** and **2** [26], meanwhile fine controlling of aggregation mode (*H* vs. *J*) in solution-processed film for improving OTFT performance is also achieved. The TFT devices have been prepared from heteroleptic triple-decker **1** and homoleptic analogue **2**, respectively, by means of solution-based quasi–Langmuir–Shäfer (QLS) method [38] and the mobilities of electrons and holes have been determined in the present work.

2. Experimental section

2.1. General

$Eu_2(Pc)[Pc(OPh)_8]_2$ and $Eu_2[Pc(OPh)_8]_3$ were prepared from the reaction between $Eu(acac)_3{\cdot}H_2O$, Li_2Pc, and $Li_2Pc(OPh)_8$, please see Electronic Supplementary Information for the detail. All other chemical reagents were purchased and used as received. Electrochemical measurement was carried out with a BAS CV-50W voltammetric analyzer. The cell comprised inlets for a glassy carbon disk working electrode of 3.0 mm in diameter and a silver-wire counter electrode. The reference electrode was Ag/Ag^+ (0.01 mol dm^{-3}), which was connected to the solution by a Luggin capillary, whose tip was placed close to the working electrode. It was corrected for junction potentials by being referenced internally to the ferrocenium/ferrocene (Fc^+/Fc) couple [$E_{1/2}$ (Fc^+/Fc) = 0.50 V vs. SCE]. Typically, a 0.1 mol dm^{-3} solution of $[Bu_4N][ClO_4]$ in CH_2Cl_2 containing 0.5 mmol dm^{-3} of sample was purged with nitrogen for 5 min, then the voltammogram was recorded at ambient temperature. The scan rate was 20 m V s^{-1}. Electronic absorption spectra were recorded with a Hitachi U-4100 spectrophotometer. For the polarized absorption spectra recording, a dichroic sheet polarizer was placed in front of the QLS films with *s*- and *p*-polarized light, respectively. The crystal data were collected on a Oxford Diffraction Gemini E diffractometer with Cu Kα radiation (λ = 1.5418 Å) at 150 K. CCDC for **2** contain the supplementary crystallographic data for this paper. These data can be obtained free of charge from the Cambridge Crystallographic Data Centre *via* www.ccdc.cam.ac.uk/data_request/cif. X-ray diffraction experiment was carried out on a Bruker AXS D8 ADVANCE X-ray diffractometer. AFM images were collected in air under ambient conditions using the tapping mode with a NanoscopeIII/Bioscope scanning probe microscope from Digital instruments.

2.2. Device fabrication

OTFT devices were fabricated on heavily doped silicon wafers with a thermally grown 300 nm thick SiO_2 layer

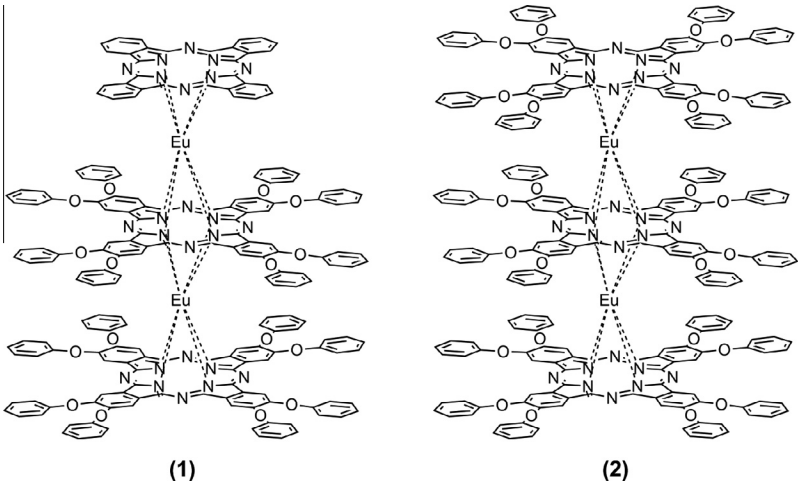

Scheme 1. Schematic structures of tris(phthalocyaninato) europium triple-decker complexes **1**–**2**.

by evaporating gold electrodes onto the QLS film employing a shadow mask. These electrodes have a channel width (W) of 28.6 mm and a channel length (L) of 0.24 mm. The ratio of the width to length (W/L) of the channel was then 119. QLS films were prepared following the method published previously [38]. Before depositing the QLS film, surface treatment for SiO_2/Si substrate was performed according to a literature method by using HMDS [39]. The electric characteristics of the devices were measured in air. The current–voltage characteristic was obtained with a Hewlett-Packard (HP) 4140B parameter analyzer at room temperature.

3. Results and discussion

3.1. Synthesis and characterization

Heteroleptic tris(phthalocyaninato) europium triple-decker complex $Eu_2(Pc)[Pc(OPh)_8]_2$ (**1**) and its homoleptic analogue $Eu_2[Pc(OPh)_8]_3$ (**2**) were prepared following the published procedures [40–43] and characterized by a series of spectroscopic methods including MALDI-TOF mass and ^{1}H NMR, Fig. S1 and S2 and Table S1 (Supplementary material). Satisfactory elemental analysis results were also obtained for both **1** and **2**, Table S1 (Supplementary material). Their sandwich-type triple-decker nature was undoubtedly elucidated by single-crystal X-ray analysis for the homoleptic species **2**.

3.2. X-ray single-crystal structure

Single crystals of $Eu_2[Pc(OPh)_8]_3$ (**2**) suitable for X-ray diffraction analysis were obtained by diffusing methanol onto the chloroform solution of this compound. Compound **2** crystallizes in the monoclinic system with the space group $P2/n$ (X-ray crystallographic data, see Table S2, (Supplementary material). Each unit cell contains two kinds of sandwich-type triple-decker molecules of **2** with very slight structural difference. As shown in Fig. 1A and B, each homoleptic triple-decker molecule is composed of two crystallographically symmetrical europium ions sandwiched by two phthalocyanine ligands and a central common phthalocyanine ligand. The europium ion is coordinated by eight isoindole nitrogen atoms. The twist angles defined as the rotation angle of one coordination square away from the eclipsed conformation of the two squares for the {[Pc(OPh)$_8$]Eu[Pc(OPh)$_8$]} subunits are 35.21° and 36.88°, respectively, in these two kinds of triple-deckers. The separations between the two N4 (isoindole) mean planes in the {[Pc(OPh)$_8$]Eu[Pc(OPh)$_8$]} subunits are 3.05 and 3.07 Å, respectively. The

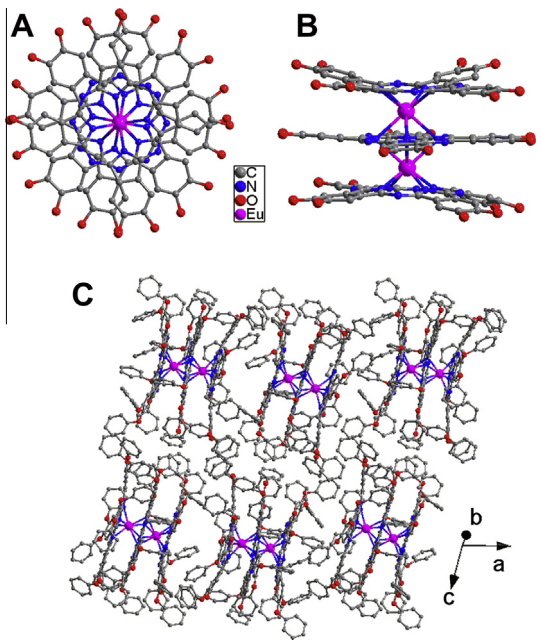

Fig. 1. Molecular structures of **2** in top view (A) and side view, (B) together with the 2D packing plot and (C) with all hydrogen atoms, benzene rings of phenoxy groups, and solvent molecules omitted for clarity.

intramolecular Eu(III) ions are separated with the distance of 3.52 and 3.53 Å, respectively. As shown in Fig. 1C, the neighboring triple-decker molecules are arranged in a slipped face-to-face mode with the separation of 12.22 Å between the nearest europium ions from different triple-decker molecules along the *a* axis, indicating the absence of π–π stacking feature between the two neighboring molecules in this direction likely due to the steric hindrance of the bulky side groups.

3.3. Electrochemical properties

Cyclic voltammetrical (CV) measurement revealed similar redox behavior for these two triple-decker complexes in CH_2Cl_2 with three reversible one-electron reduction couples and three or four one-electron oxidations observed in the range from −1.7 to + 1.8 V, Table 1 and Fig. 2. According to the first oxidation half-wave potential, +0.59 and +0.68 V for **1** and **2**, respectively, the HOMO energy level is therefore estimated to be −5.03 and −5.12 eV for **1** and **2** [44]. This, obviously, matches well with the work function of gold (−5.1 eV) and therefore ensures the facilitation of the hole injections from the Au electrodes to the phthalocyanine-based semiconductors. Nevertheless, the LUMO energies are approximately −4.02 and −4.03 eV for **1** and **2** deduced from their first reduction half-wave potentials, −0.42 V for **1** and −0.41 V for **2**, Table 1, which just locate within the range required for air-stable *n*-type OTFT materials [24,45]. These results reveal the air-stable ambipolar organic semiconducting nature of these two triple-decker compounds and their potential in OTFT devices. In addition, compound **2** is very slightly easier to reduce than **1**, by about 0.01 V for E_{red1} and E_{red2}, and 0.03 V for E_{red3}, but slightly more difficult to oxidize, by 0.09, 0.05 and 0.02 V for E_{oxd1}, E_{oxd2} and E_{oxd3}, respectively, in accordance with the presence of additional peripheral electron-withdrawing phenoxy substituents on **2.**

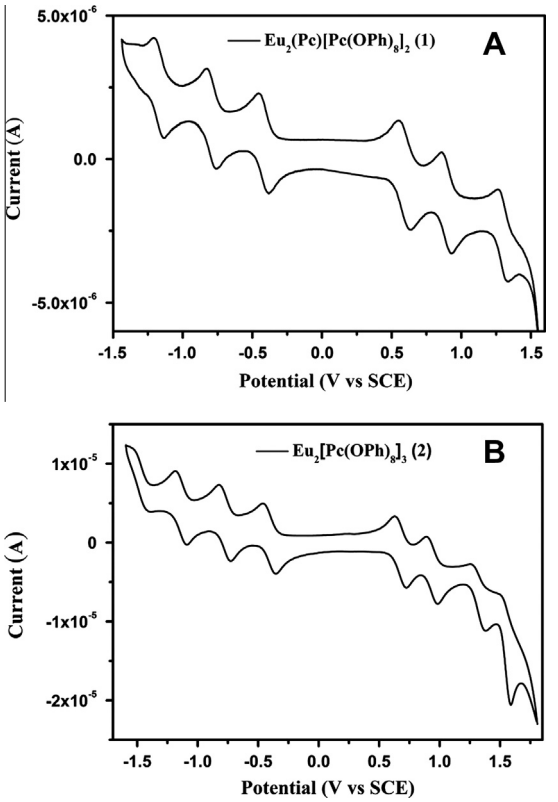

Fig. 2. Cyclic voltammogram (CV) of compounds **1**–**2** (A–B) in CH_2Cl_2 containing 0.1 mol dm^{-3} $[Bu_4N][ClO_4]$ at a scan rate of 20 m V s^{-1}.

3.4. OTFTs characterization

OTFT devices were fabricated with a top-contact device configuration on hexamethyldisilazane (HMDS)-modified SiO_2 (300 nm)/Si substrates using the QLS technique. Gold (Au) was used as drain and source electrodes. All the TFT measurements were performed under ambient atmosphere. Experimental data were analyzed using standard field-effect transistor equations: $I_{ds} = (W/2L)\mu C_0(V_g - V_{th})^2$, where I_{ds} is the source-drain current, V_g is the gate voltage, C_0 is the capacitance per unit area of the dielectric layer, and V_{th} is the threshold voltage, and μ is the mobility n the saturation region [46]. The mobility (μ) and threshold voltage (V_{th}) can then be calculated from the slope and intercept of the linear part of the V_g vs. $(I_{ds})^{1/2}$ plot (at $V_{ds} = 40$ or −40 V), respectively. As summarized in Table S3 (Supplementary material) and shown in Fig. 3A, the devices based on the QLS film of heteroleptic triple-decker **1** measured in air present carrier mobility not only for hole but also for electron with average value of 0.68 and 0.014 $cm^2 V^{-1} s^{-1}$ for **1**, respectively, revealing the typical ambipolar semiconductor nature of the this compound. This is also true for the devices fabricated from homoleptic analogue **2** but with significantly lower electron and hole mobilities in the range of 0.041–0.0026 $cm^2 V^{-1} s^{-1}$, Fig. 3B. It is worth noting that the devices fabricated from **1** seem to exhibit the best ambipolar performance in terms of the charge mobilities for both electron and hole among the solution-processed phthalocyanine-based semiconductors reported thus far [35]. This is hard to imagine for devices with amorphous-like thin film nature that have been fabricated from small molecular organic semiconduc-

Table 1
Half-wave redox potentials of $Eu_2(Pc)[Pc(OPh)_8]_2$ (1) and $Eu_2[Pc(OPh)_8]_3$ (2) (V vs. SCE) in CH_2Cl_2 containing 0.1 mol dm^{-3} $[Bu_4N][ClO_4]$ together with the HOMO and LUMO levels of compounds **1** and **2**.

Complex	Red_3/V	Red_2/V	Red_1/V	Oxd_1/V	Oxd_2/V	Oxd_3/V	Oxd_4/V	E_{HOMO}/eV[a]	E_{LUMO}/eV[a]	$\Delta E^\circ_{1/2}$/V[b]
1	−1.17	−0.79	−0.42	0.59	0.89	1.30	–	−5.03	−4.02	1.01
2	−1.14	−0.78	−0.41	0.68	0.94	1.32	1.55	−5.12	−4.03	1.09

[a] Calculated from empirical formula of HOMO = −(Oxd_1 + 4.44 eV); LUMO = −(Red_1 + 4.44 eV) [19].
[b] $\Delta E^\circ_{1/2} = Oxd_1 - Red_1$, i.e. the HOMO LUMO gap of corresponding molecule.

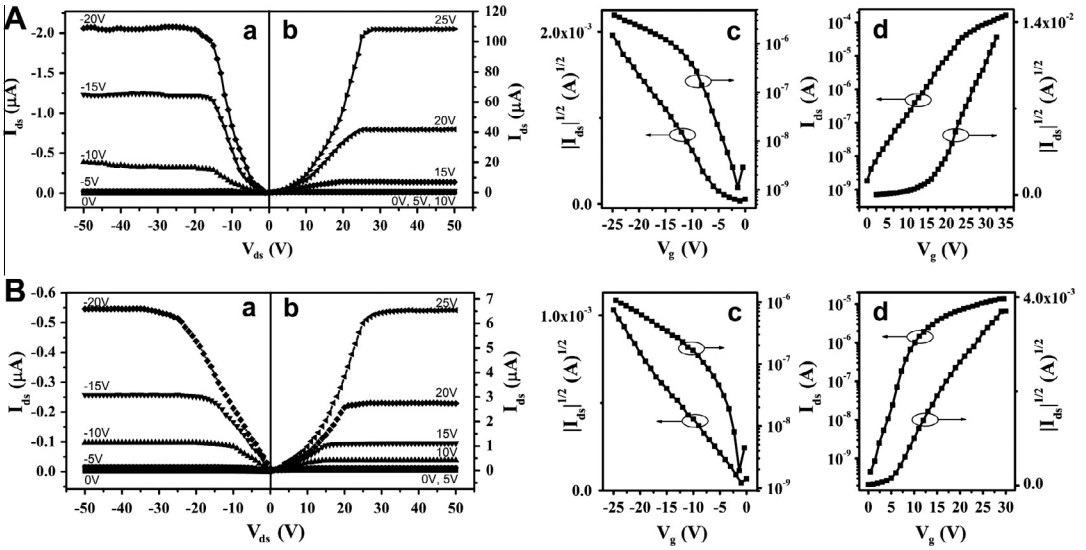

Fig. 3. Output characteristics (I_{ds} vs. V_{ds}) and transfer characteristics ($|I_{ds}|^{1/2}$ vs. V_g) of ambipolar OTFT device based on QLS films of **1** (A) and **2** (B) deposited on HMDS-treated SiO_2/Si (300 nm) substrate with Au top contacts measured in air. Current–voltage output plots with various Vg for *p*-channel (a) and for *n*-channel (b) and the transfer characteristics of OTFTs at V_{ds} = −40 V for *p*-channel (c) and V_{ds} = +40 V for *n*-channel (d).

tor based on solution deposition method [47,48], suggesting the great potential of sandwich-type tri(phthalocyaninato) europium complexes for applications in low-cost and large-area organic electronics. Nevertheless, the OTFTs of **1** exhibit negligible variation in both electron and hole mobilities after 4 months stored under ambient without exclusion of light or humidity, Fig. S3 (Supplementary material), indicating the good stability of the devices in air.

For the purpose of clarifying the far larger charge mobilities of heteroleptic triple-decker **1** relative to its homoleptic analogue **2,** analysis over the internal film structure of both compounds have been conducted on the basis of thin-film XRD, and AFM techniques (*vide infra*). Before that, however, we measured the electronic absorption and polarized UV–vis spectra to obtained an insight into the molecular packing mode of the triple decker molecules.

3.5. Electronic absorption and polarized UV–vis spectra

As shown in Fig. 4, compounds **1** and **2** in $CHCl_3$ display intense Q band at 651 and 664 nm, respectively, which takes dramatic blue-shift in comparison with that of monomeric phthalocyaninato metal complexes as examplified by 2,3,9,10,16,17,23,24-octaphenoxyphthalocyaninato zinc complex at 680 nm in $CHCl_3$ [39], indicating the intense intramolecular π–π interaction among the three face-to-face stacked phthalocyanine rings in the triple-decker molecule for both compounds [31–33]. However, after being fabricated into the QLS films, the main Q band was broadened and blue-shifted to 640 nm for **1** but red-shifted to 673 nm for **2**, indicating the formation of *H*-aggregation-type and *J*-aggregation-type molecular packing structure in the QLS films of **1** and **2**, respectively, on the basis of exciton theory [49] and previously published results [40–43,50–53]. This is also supported by the orientation angle (dihedral angle) revealed for the

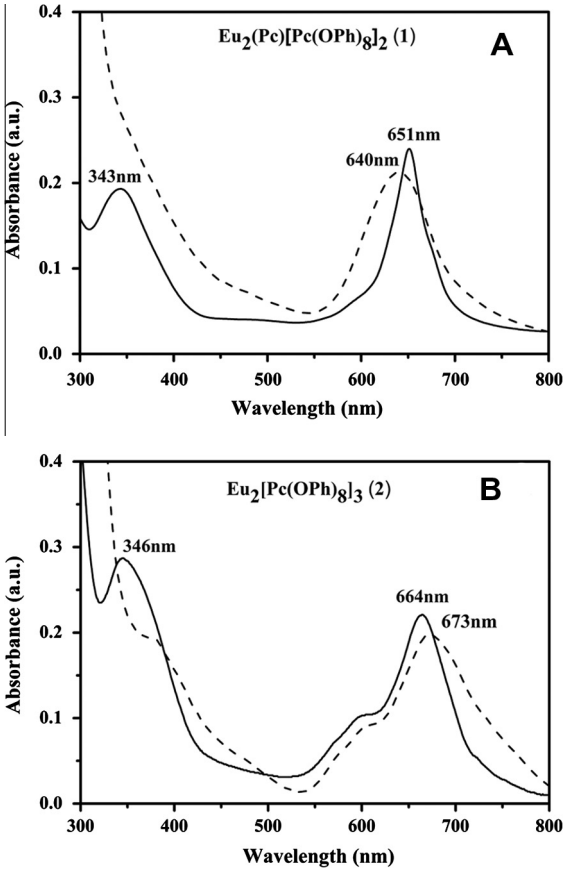

Fig. 4. UV–vis absorption spectra of compounds **1–2** (A,B) in dilute chloroform solution (solid line) and QLS films (dash line).

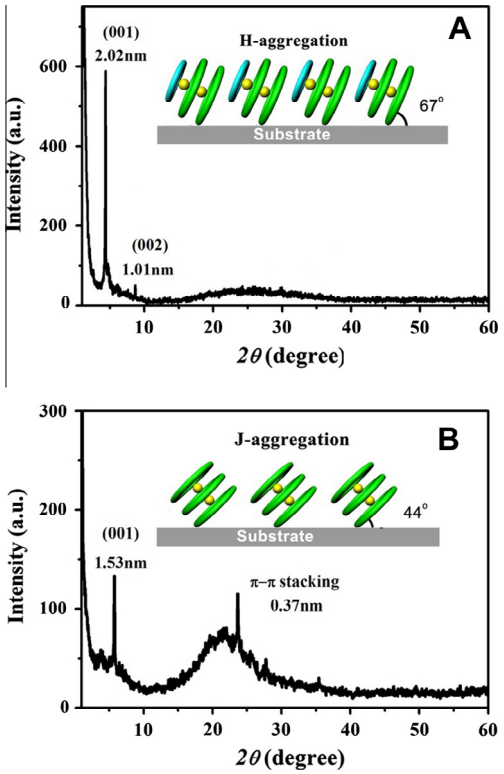

Fig. 5. X-ray diffraction patterns of the QLS films of compounds **1–2** (A,B) on glass substrate.

phthalocyanine ring with respect to the substrate (66.3° for **1** and 42.3° for **2**) according to polarized UV–vis measurement [48], Fig. S4 and Table S4 (Supplementary material). Obviously, the much more effective intermolecular face-to-face interaction in the *H*-aggregates for heteroleptic triple-decker **1** than that in the *J*-aggregation of homoleptic triple-decker analogue **2** is able to provide the π electrons (as well as holes) with an extensive area for delocalization, which in turn is responsible for the much larger carrier mobilities revealed for the devices fabricated from the former compound than the latter one [54,55].

3.6. Film microstructures and morphologies

The quality of the thin solid films, it is in fact the information concerning the molecular ordering in the film, could be assessed using X-ray diffraction technique. As shown in Fig. 5A, the out-of-plane (OOP) XRD diagram of QLS films of **1** deposited on glass substrate shows two well-defined low-angle diffraction peaks at $2\theta = 4.38°$ and 8.70°, which are ascribed to the diffractions from the (001) and (002) planes, respectively, indicating the long-range molecular ordering across the thickness of the QLS films [37,56]. The OOP *d*-spacing calculated according to the Bragg equation is about 2.02 nm, which corresponds to a periodic distance between two adjacent triple-decker molecules of **1** along the direction of the substrate surface normal. Judging from the diagonal dimension of the $Eu_2[Pc(OPh)_8]_3$ molecule, 2.20 nm, on the basis of single crystal X-ray diffraction result, the orientation angle between the phthalocyanine ring in the triple-decker molecule and substrate surface of ca. 66.7° is deduced. This result is obviously in good accordance with that deduced from polarized UV–vis spectroscopic measurement, revealing that the triple-decker molecules of **1** are oriented nearly perpendicular to the substrate surface in a face-to-face stack [49]. It is noteworthy that the fact that only (00*l*) diffraction peaks are observed for the films of **1** but without giving obvious peak for the π–π stacking in the OOP XRD diagram suggests the identical edge-on orientation employed by the molecules of **1** on the substrate with the π–π stacking direction parallel to the substrate [26]. This, in combination with the long-range ordering nature of the molecular stacking in the thin film state, leads to a corresponding decrease in the barrier of charge transport over the QLS films, which in turn contributes to the excellent charge carrier mobility as revealed for the devices fabricated from **1**. In contrast, the QLS films fabricated from $Eu_2[Pc(OPh)_8]_3$ (**2**) exhibit substantial inclination in molecular orientation with an estimated tilt angle of ~44.1° according to the peak at $2\theta = 5.76°$ in the OOP XRD diagram of QLS films of **2**, Fig. 5B. This defines a smaller OOP *d*-spacing of 1.53 nm than that for **1**, therefore confirming the *J*-aggregate mode nature for the QLS films of **2** [50,51,57,58]. Interestingly, an additional strong peak

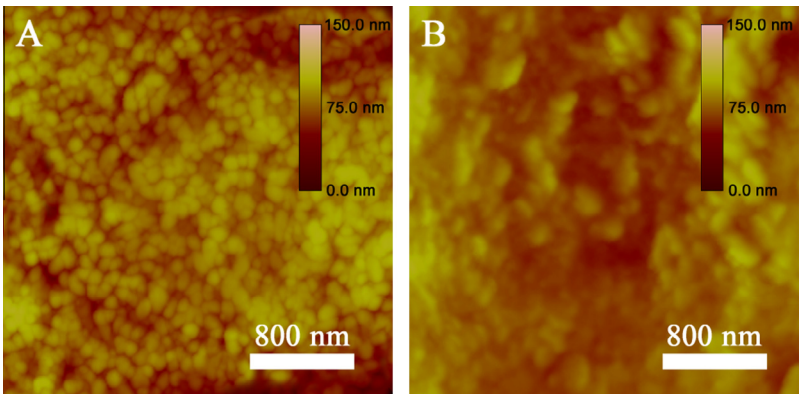

Fig. 6. AFM images of the QLS films of compounds **1-2** (A,B) deposited on HMDS-treated SiO_2/Si substrates.

was also observed for the QLS films of **2** at $2\theta = 23.66^{\circ}$ (corresponding to 0.37 nm), which can be attributed to the formation of π–π stacking among tetrapyrrole rings of triple-decker molecules with the face-on orientation [59,60]. Obviously, as a result of the change in molecular packing from *H*-aggregation for **1** to *J*-aggregation for **2**, the crystalline packing in the QLS films changes from an identical edge-on configuration for the former compound to both the face-on and edge-on characters for the latter one. The strong face-to-face intra- and in particular intermolecular π–π interactions between the phthalocyanine rings of **1** then induce the formation of the QLS films with corresponding texture. As revealed by the atomic force microscope (AFM), Fig. 6A, the thin film of **1** shows nano-sized grains (ca.80–100 nm in diameter) without large grain boundaries and special separation on the HMDS-treated substrate surface. This is in good contrast to the disconnected grains (100–500 nm in length) with large gaps and cracks between aggregate domains observed for the QLS film of **2**, Fig. 6B. Unlike the situation for heteroleptic triple-decker compound **1**, the nano-sized grain discontinuity in the QLS film of homoleptic analogue **2** will surely add negative effect on the carrier mobility for the OTFT devices fabricated.

4. Conclusions

In summary, two heteroleptic and homoleptic tris(phthalocyaninato) europium triple-decker complexes bearing different number of peripheral electron-withdrawing phenoxy substituents were designed and synthesized. Measurements over the OTFT devices fabricated from these two sandwich compounds by solution-based QLS method reveal their ambipolar semiconductor nature associated with suitable HOMO and LUMO energy levels. Due to the *J*-aggregation mode employed by the homoleptic triple-decker molecules in the QLS film, significantly lower carrier mobilities with the values of 0.041 and 0.0026 $cm^2 \cdot V^{-1} s^{-1}$ for electron and hole, respectively, have been revealed for the TFT devices of homoleptic triple-decker, in comparison with those of 0.68 and 0.014 $cm^2 V^{-1} s^{-1}$ for heteroleptic analogue with the *H*-aggregation mode in the QLS film. The latter of which is among the highest ones achieved so far for solution-processable single-component phthalocyanine-based TFTs obtained under ambient conditions. Most importantly, the performance of the TFT devices fabricated from the heteroleptic triple-decker 1 remain stable in terms of both the carrier mobilities and on/off ratio even after having been put in air for 4 months. These results are helpful for further design and preparation of ambipolar semiconductor materials with improved device performance.

Acknowledgements

We thanks for financial support from the National Key Basic Research Program of China (Grant Nos. 2013CB933402 and 2012CB224801), Natural Science Foundation of China (20871055), and the Natural Science Foundation of Shandong Province (ZR2011BZ005).

Appendix A. Supplementary material

Supplementary data associated with this article can be found, in the online version, at http://dx.doi.org/10.1016/j.orgel.2013.07.003.

References

[1] C.D. Dimitrakopoulos, P.R.L. Malenfant, Adv. Mater. 14 (2002) 99.
[2] H. Sirringhaus, Adv. Mater. 17 (2005) 2411.
[3] R. Li, W. Hu, Y. Liu, D. Zhu, Acc. Chem. Res. 43 (2010) 29.
[4] H. Usta, A. Facchetti, T.J. Marks, Acc. Chem. Res. 44 (2011) 501.
[5] W. Wu, Y. Liu, D. Zhu, Chem. Soc. Rev. 39 (2010) 1489.
[6] R.P. Ortiz, A. Facchetti, T.J. Marks, Chem. Rev. 110 (2010) 205.
[7] S. Liu, W.M. Wang, A.L. Briseno, S.C.B. Mannsfeld, Z. Bao, Adv. Mater. 21 (2009) 1217.
[8] Y. Wang, Y. Chen, R. Li, S. Wang, X. Li, J. Jiang, Langmuir 23 (2007) 5836.
[9] C.R. Newman, C.D. Frisbie, D.A. da Silva, J.L. Bredas, P.C. Ewbank, K.R. Mann, Chem. Mater. 16 (2004) 4436.
[10] J. Zaumseil, H. Sirringhaus, Chem. Rev. 107 (2007) 1296.
[11] A. Facchetti, Mater. Today 10 (2007) 28.
[12] Z. Chen, Y. Zheng, H. Yan, A. Facchetti, J. Am. Chem. Soc. 131 (2009) 8.
[13] H. Yan, Z. Chen, Y. Zheng, C. Newman, J.R. Quinn, F. Döotz, M. Kastler, A. Facchetti, Nature 457 (2009) 67.
[14] M.M. Durban, P.D. Kazarinoff, C.K. Luscombe, Macromolecules 43 (2010) 6348.
[15] L.L. Chua, J. Zaumseil, J.F. Chang, E.C.-W. Ou, P.K.–H. Ho, H. Sirringhaus, R.H. Friend, Nature 434 (2005) 194.
[16] F.S. Kim, E. Ahmed, S. Subramaniyan, S.A. Jenekhe, ACS Appl. Mater. Interface 2 (2010) 2974.
[17] K. Walzer, B. Maennig, M. Pfeiffer, K. Leo, Chem. Rev. 107 (2007) 1233.
[18] M.A. Baldo, M.E. Thompson, S.R. Forrest, Nature 403 (2000) 750.
[19] M.A. Baldo, D.F. O'Brien, Y. You, A. Shoustikov, S. Sibley, M.E. Thompson, S.R. Forrest, Nature 395 (1998) 151.
[20] A. Dodabalapur, H.E. Katz, L. Torsi, R.C. Haddon, Science 269 (1995) 1560.
[21] R. Ye, M. Baba, K. Suzuki, K. Mori, Solid State Electron 52 (2008) 60.
[22] J. Wang, H. Wang, X. Yan, H. Huang, D. Yan, Appl. Phys. Lett. 87 (2005) 093507.
[23] T. Yasuda, T. Tsutsui, Chem. Phys. Lett. 402 (2005) 395.
[24] B.A. Jones, A. Facchetti, M.R. Wasielewski, T.J. Marks, J. Am. Chem. Soc. 129 (2007) 15259.
[25] M.L. Tang, J.H. Oh, A.D. Reichardt, Z. Bao, J. Am. Chem. Soc. 131 (2009) 3733.
[26] H. Usta, C. Risko, Z. Wang, H. Huang, M.K. Deliomeroglu, A. Zhukhovitskiy, A. Facchetti, T.J. Marks, J. Am. Chem. Soc. 131 (2009) 5586.
[27] X. Guo, R.P. e Ortiz, Y. Zheng, Y. Hu, Y.-Y. Noh, K.-J. Baeg, A. Facchetti, T.J. Marks, J. Am. Chem. Soc. 133 (2011) 1405.
[28] E.J. Meijer, D.M. de Leeuw, S. Setayesh, E. van Veenendaal, B.-H. Huisman, P.W.M. Blom, J.C. Hummelen, U. Scherf, T.M. Klapwijk, Nat. Mater. 2 (2003) 678.
[29] D.T. Chase, A.G. Fix, S.J. Kang, B.yD. Rose, C.D. Weber, Y. Zhong, L.N. Zakharov, M.C. Lonergan, C. Nuckolls, M.M. Haley, J. Am. Chem. Soc. 134 (2012) 10349.
[30] C. Wang, H. Dong, W. Hu, Y. Liu, D. Zhu, Chem. Rev. 112 (2012) 2208.
[31] J. Jiang, K. Kasuga, D.P. Arnold, in: H.S. Nalwa (Ed.), Supramolecular Photosensitive and Electroactive Materials, Academic Press, New York, 2001 (Ch. 2).
[32] J. Jiang, D.K.P.F. Ng, Acc. Chem. Res. 42 (2009) 79.
[33] Y. Chen, W. Su, M. Bai, J. Jiang, X. Li, Y. Liu, L. Wang, S. Wang, J. Am. Chem. Soc. 127 (2005) 15700.
[34] G. Guillaud, M.A. Sadoun, M. Maitrot, J. Simon, M. Bouvet, Chem. Phys. Lett. 167 (1990) 503.
[35] J. Kan, Y. Chen, D. Qi, Y. Liu, J. Jiang, Adv. Mater. 24 (2012) 1755.
[36] G. Lu, M. Bai, R. Li, X. Zhang, C. Ma, P.-C. Lo, D.K.P. Ng, J. Jiang, Eur. J. Inorg. Chem. 18 (2006) 3703.
[37] Y. Chen, D. Li, N. Yuan, J. Gao, R. Gu, G. Lu, M. Bouvet, J. Mater. Chem. 22 (2012) 22142.
[38] Y. Chen, M. Bouvet, T. Sizun, Y. Gao, C. Plassard, E. Lesniewska, J. Jiang, Phys. Chem. Chem. Phys. 12 (2010) 12851.
[39] S.E. Maree, T. Nyokong, J. Porphyrins Phthalocyanines 5 (2001) 782.
[40] D.K.P. Ng, J. Jiang, Chem. Soc. Rev. 26 (1997) 433.
[41] W. Liu, J. Jiang, N. Pan, D.P. Arnold, Inorg. Chim. Acta 310 (2000) 140.

[42] L.A. Lapkina, E. Niskanen, H. Rönkkömäki, V.E. Larchenko, K.I. Popov, A.Y. Tsivadze, J. Porphyrins Phthalocyanines 4 (2000) 588.
[43] Y. Zhang, W. Jiang, J. Jiang, Q. Xue, J. Porphyrins Phthalocyanines 11 (2007) 100.
[44] SCE energy level is taken to be −4.44 eV below the vacuum level, for detail please see A.J. Bard, L.R. Faulkner, in: Electrochemical Methods-Fundamentals and Applications, Wiley, New York, 1984.
[45] Z. Wang, C. Kim, A. Facchetti, T.J. Marks, J. Am. Chem. Soc. 129 (2007) 13362.
[46] S.M. Sze, Physics of Semiconductor Devices, John Wiley & Sons, New York, 1981.
[47] P.M. Beaujuge, J.M.J. Fréchet, J. Am. Chem. Soc. 133 (2011) 20009.
[48] Y. Qiao, Y. Guo, C. Yu, F. Zhang, W. Xu, Y. Liu, D. Zhu, J. Am. Chem. Soc. 134 (2012) 4084.
[49] M. Kasha, H.R. Rawls, M.A. El-Bayoumi, Pure Appl. Chem. 11 (1965) 371.
[50] Y. Chen, H. Liu, P. Zhu, Y. Zhang, X. Wang, X. Li, J. Jiang, Langmuir 21 (2005) 11289.
[51] Y. Chen, R. Li, R. Wang, P. Ma, S. Dong, Y. Gao, X. Li, J. Jiang, Langmuir 23 (2007) 12549.
[52] M. Kimura, T. Kuroda, K. Ohta, K. Hanabusa, H. Shirai, N. Kobayashi, Langmuir 19 (2003) 4825.
[53] G. Lu, Y. Chen, Y. Zhang, M. Bao, Y. Bian, X. Li, J. Jiang, J. Am. Chem. Soc. 130 (2008) 11623.
[54] J.E. Anthony, J.S. Brooks, David L. Eaton, S.R. Parkin, J. Am. Chem. Soc. 123 (2001) 9482.
[55] J. Locklin, K. Shinbo, K. Onishi, F. Kaneko, Z. Bao, R.C. Advincula, Chem. Mater. 15 (2003) 1404.
[56] T.J. Prosa, M.J. Winokur, J. Moulton, P. Smith, A.J. Heeger, Macromolecules 25 (1992) 4364.
[57] E.H.A. Beckers, S.C.J. Meskers, A.P.H.J. Schenning, Z. Chen, F. Würthner, P. Marsal, D. Beljonne, J. Cornil, R.A.J. Janssen, J. Am. Chem. Soc. 128 (2006) 649.
[58] S. Kim, T.K. An, J. Chen, I. Kang, S.H. Kang, D.S. Chung, C.E. Park, Y.-H. Kim, S.-K. Kwon, Adv. Funct. Mater. 21 (2011) 1616.
[59] J. Rivnay, R. Steyrleuthner, L.H. Jimison, A. Casadei, Z. Chen, M.F. Toney, A. Facchetti, D. Neher, A. Salleo, Macromolecules 44 (2011) 5246.
[60] N. An, Y. Shi, J. Feng, D. Li, J. Gao, Y. Chen, X. Li, Org. Electron. 14 (2013) 1197.